RESEARCH   **Open Access**

A Finite Element-Based Methodology for the Thermo-mechanical Analysis of Early Age Behavior in Concrete Structures

H. Cifuentes[1*] , F. Montero-Chacón[2], J. Galán[3], J. Cabezas[4] and A. Martínez-De la Concha[1]

Abstract

This paper presents a general procedure based on fracture mechanics models in order to analyze the level of cracking and structural safety in reinforced concrete elements at early ages, depending on the stripping time. Our procedure involves the development of a thermo-mechanical numerical model based on the finite element method that accounts for the change in the mechanical properties of concrete with time. Moreover, fracture mechanisms are analyzed by means of a material damage model, which is characterized via specific experimental results obtained for standard specimens and notched beams under three-point bending testing. The loading conditions are both thermal and mechanical, and are obtained from the hydration process for a given concrete dosage. The presented methodology allows for the determination of the optimal stripping time, whereas it helps assessing the analysis of the cracking and the stress states of the elements under consideration. A practical application, namely the analysis of a retaining wall, is used to validate our methodology, showing its suitability in engineering practice.

Keywords: heat of hydration, early age cracking, thermo-mechanical model, fracture mechanics of concrete

1 Introduction

Concrete mechanical behavior at early age is characterized by the development of low mechanical properties and the appearance of thermal stresses generated by temperature gradients from the heating process during the cement hydration (Wang and Luan 2018). Moreover, along with the exothermal reaction, material shrinkage takes place. This phenomenon can generate the so-called early-age cracking in concrete, which can be extremely harmful if a premature application of the load is performed (Mihashi and Leite 2004). On the other hand, the correct choice of the stripping time of an on-site cast in place concrete structure results in significant savings in the implementation of the structure (i.e., cost and time), with the structural safety factors depending on the

chosen time and the lack of excessive cracking level in the material.

For a proper analysis of concrete at early ages, the evolution of the thermal, mechanical, and fracture properties of the material must be known (Bergström and Byfors 1980; Lee et al. 2016), as well as the relationship between them. This issue, then, promotes having a complete picture of the behavior of concrete in a period of time close to the pouring age (Faria et al. 2006). In this work a numerical model has been developed in order to estimate the optimal time for removing the formwork without damaging the structure. In addition, the model also provides the maximum load that a structure of concrete can support at a certain age. This fact is very important during the on-site execution, where time plays a crucial role and should be diminished as much as possible (Wu et al. 2011). Traditionally, structural health monitoring (SHM) systems have focused on monitoring the conditions of the concrete using external techniques based on accelerometers or displacement transducers, among others (Park and Yim 2017). Moreover, monitoring the internal properties of concrete requires the development of

*Correspondence: bulte@us.es
[1] Dpto. Mecánica de Medios Continuos y Teoría de Estructuras, ETS de Ingeniería, Universidad de Sevilla, Seville, Spain
Full list of author information is available at the end of the article

Cifuentes *et al. Int J Concr Struct Mater*   (2019) 13:41

Page 2 of 20

embedded sensors so as to gather data during the curing stage (Newell and Goggins 2018). In this sense, in order to measure the temperature in the concrete and characterize the curing process from the first pour, an embedded sensor was designed. The monitoring framework addresses aspects related to sensing, local wired transmission, data storage, and visualization.

Furthermore, a numerical model has been developed in order to assess the cracking level and stress states in terms of the stripping time. More precisely, the model takes into account the thermal processes taking place during the cement hydration and has been characterized and verified experimentally with laboratory specimens (e.g., standard specimens and notched beams) and large structures, respectively. The model also accounts for the evolution of mechanical properties with time, as well as the fracture mechanisms via cohesive elements. Service loading conditions are based on the heat of hydration for a given concrete dosage. Although other reliable numerical models can be found in the literature (Kwan and Ma 2017; Lee and Kim 2009), the most of them are mainly focused on the behavior of the material and the methodology described in this work presents an eminently practical purpose but considering the different advanced approaches involved in the early age behavior of concrete structures, from the chemical reactions produced during the evolution of the hydration of the cement to the macroscopic analysis of the concrete structure, with in situ measurements, by using fracture mechanics models based on bi-linear cohesive laws of concrete in tension at early ages.

The methodology herein described is very complete and different from other similar methodologies that can be found in the bibliography since it integrates all the different analyzes carried out in this work in the design process of a concrete structure, from the set-up of the numerical models, the experimental verification and validation in laboratory and the application in a real structure. This methodology considers the analysis of the experimental evolution of the mechanical properties of concrete at early age and its relationship with the developed temperature, which can be easily measured in situ, through thermo-chemical–mechanical models (Schindler and Folliard 2005). Likewise, the mechanical behavior of concrete structures was analyzed by numerical models based on the fracture mechanics of concrete, using cohesive laws for its tensile behavior that evolve with the age of the material. However, the procedure is of a very simple work application, requiring only the measurement of the temperature as the control parameter to be compared with the numerical predictions and to check whether the hydration of cement is taking place correctly.

The methodology presented in this work has been applied in a real case such as a slender retaining wall in Loja (Granada, Spain), allowing the determination of the optimal stripping time and providing an assessment of the cracking and stress states of these elements during the construction process, proving its validity. It must be remarked that, as pointed out by Mihashi and Leite, the potential damage generated during the hydration processes in large concrete structures can be harmful for their durability; thus, new methodologies for the control of early age cracking are essential to ensure the sustainability of these types of structures (Mihashi and Leite 2004).

2 Methodology

The main objective of the model is to analyze the thermo-mechanical behavior of concrete structures at early ages in order to determine the optimal stripping time while providing a proper security level in compliance to the serviceability limit state (SLS). Therefore, the numerical model presented herein takes into account the evolution of material properties with age, the hydration process, the thermally-induced stresses, the evolutionary construction phases, and the total elapsed loading time. In this section, we present the thermal model that is used to analyze the hydration process and the mechanical model that is used to analyze the thermo-mechanical stresses resulting from the former phenomenon.

2.1 Analysis of the Heat of Hydration

The starting point of the thermo-mechanical model is the analysis of the cement hydration process (Ulm and Coussy 1995). Thus, in order to include this into the methodology, it is necessary to account for the heat flux that evolves with the curing period. Although there are several models available in the literature (Bernard et al. 2003; Hattel and Thorborg 2003; Wang and Lee 2010), the model used to predict the flow of the heat of hydration is that from Schindler and Folliard (Schindler and Folliard 2005) because of its simplicity and dependence on the type of cement and concrete composition.

Schindler and Folliard proposed a novel method in order to quantify the heat flux transferred to the concrete mix and originated by the hydration of the cement. According to this method, the total heat of hydration of a Portland cement class is a function of the heat of hydration provided by its components, which is given by:

$$H_{cem} = 500p_{C_3S} + 260p_{C_2S} + 866p_{C_3A} + 420p_{C_4AF} + 624p_{SO_3} + 1186p_{FreeCaO} + 850p_{MgO}$$

$$(1)$$

where H_{cem} is the total heat of hydration of the Portland cement (J/g) considering fully-hydrated cement and p_i is

the mass of the i-th component to the total cement ratio. Table 1 shows the components of cement classes I and II (Poole 2007).

The progress of the hydration of Portland cement can be quantified by the so-called degree of hydration, δ, which varies from 0 to 1 (with 1 indicating a complete hydration). This degree of hydration is defined as the ratio of the heat transferred at a given time t, $H(t)$ in J/g, to the total amount of heat in the reaction (van Breugel 1998):

$$\delta(t) = \frac{H(t)}{H_u} \tag{2}$$

with H_u the total heat available for the hydration reaction, $H_u = H_{cem}$.

The degree of hydration is usually modelled using an exponential curve with the following mathematical expression:

$$\delta(t_e) = \delta_u e^{-\left(\frac{\tau}{t_e}\right)^{\beta}} \tag{3}$$

where δ_u is the total degree of hydration, β is the hydration shape parameter, τ is the hydration time parameter (in hours), and t_e is the equivalent age (in hours) at the reference temperature, T_r (K), which is given by:

$$t_e(t) = \sum_0^t e^{\left[-\frac{E_a}{R}\left(\frac{1}{T_r} - \frac{1}{T}\right)\right]} \Delta t \tag{4}$$

where Δt is the time interval (in hours), T is the average temperature of the concrete mix (in K), R is the universal gas constant (8.314 J/mol/K), and E_a is the activation energy (J/mol) defined as proposed in (Schindler and Folliard 2005) which is in accordance to Arrhenius theory.

Once these parameters are calculated, the rate of the heat generation due to the hydration process, Q_h, can be obtained as:

$$Q_h(t) = H_u W_c \left[\left(\frac{\tau}{t_e}\right)^{\beta}\left(\frac{\beta}{t_e}\right)\delta(t_e)\right] e^{\left[-\frac{E_a}{R}\left(\frac{1}{T_r} - \frac{1}{T}\right)\right]}. \tag{5}$$

where W_c is the cement content (kg/m^3). A detailed description of the model can be found in (Schindler and Folliard 2005; van Breugel 1998).

The heat equation, which can be solved by means of the finite element method (FEM), is then used to determine the evolution of the temperature in the concrete mix at any instant t by:

$$\rho c_p \frac{\partial T}{\partial t} - \nabla(k\nabla T) = Q_h \tag{6}$$

where ρ is the density, c_p is the specific heat, k is the thermal conductivity, and the source term is the volumetric heat flux as defined in Eq. (5).

As mentioned above, Eq. (6) is solved by means of the FEM in order to determine the temperature of the concrete mix at any point of the domain and at any instant within the curing period. This temperature field is consequently used by the thermo-mechanical model in order to evaluate the mechanical properties and determine the thermal stresses that may induce early age cracking. Convective and radiative boundary conditions are considered by accounting for their corresponding heat fluxes, q_{cv} and q_{rd}, respectively, as:

$$q_{cv} = h(T_{cv} - T_r) \tag{7}$$

$$q_{rd} = \sigma \in \left(T_{rd}^4 - T_r^4\right) \tag{8}$$

where h is the film coefficient between concrete and air, T_{cv} is the temperature of the convective boundary, T_r is the radiant room temperature, σ is the Stefan-Boltzmann constant, $\in$ is the emissivity, and T_{rd} is the temperature of the radiative boundary.

2.2 Thermo-mechanical Model

Since the numerical model has to provide the stress and cracking states in the material produced by the hydration process, along with other mechanical loads, a thermo-mechanical model has to be defined (Cifuentes and Karihaloo 2018). Consequently, the model should also consider the evolution of material properties with age. Thus, the so-called concrete damage plasticity (CDP) model, developed by Lubliner et al. (1989), and with modifications by Lee and Fenves (1998), is used in this work. The CDP model has proven capabilities for the analysis of fracture in concrete specimens and structures (Cifuentes and Karihaloo 2018; Montero-Chacón et al. 2015, 2017).

Table 1 Weight fractions of the components of cement classes I and II to the total cement ratio.

Class	C$_3$S	C$_2$S	C$_3$A	C$_4$AF	FreeCaO	SO$_3$	MgO
I	0.565	0.140	0.100	0.080	0.029	0.035	0.013
II	0.51	0.24	0.053	0.166	0.004	0.025	0.009

The continuum damage model formulation in elasticity (Kachanov 1980; "Continuum damage mechanics: Part I-General concepts" 1988) reads as follows:

$$\boldsymbol{\sigma} = (1 - d)\mathbf{D}_0^{el} : \boldsymbol{\varepsilon}^{el} \tag{9}$$

where $\boldsymbol{\sigma}$ is the Cauchy stress tensor, d is the damage variable, $\mathbf{D}_0^{el}$ is the original (i.e., undamaged) elastic stiffness tensor, and $\boldsymbol{\varepsilon}^{el}$ is the elastic strain.

The total strain tensor in concrete, $\boldsymbol{\varepsilon}$, can be split into the instantaneous reversible elastic strain, $\boldsymbol{\varepsilon}^{el}$, the irreversible inelastic strain, $\boldsymbol{\varepsilon}^{in}$, the creep strain, $\boldsymbol{\varepsilon}^c$, the shrinkage strain, $\boldsymbol{\varepsilon}^s$, and the thermal expansion strain, $\boldsymbol{\varepsilon}^{th}$ (Bazant 1988):

$$\boldsymbol{\varepsilon} = \boldsymbol{\varepsilon}^{el} + \boldsymbol{\varepsilon}^{in} + \boldsymbol{\varepsilon}^c + \boldsymbol{\varepsilon}^s + \boldsymbol{\varepsilon}^{th} \tag{10}$$

The creep strain at the instant $t > t_0$ for those cases where concrete is loading at t_0, can be considered as a reduction of the Young's modulus through the creep coefficient as follows (Neville 1995):

$$\boldsymbol{\varepsilon}^c = \frac{\sigma_c(t_0)}{E_{ci}} \cdot \varphi(t, t_0). \tag{11}$$

The creep coefficient, $\varphi(t, t_0)$, can be calculated in different ways. In this paper, it was determined according to the Model Code formulations (fib CEB-FIP 2012), considering the specific type of cement employed in the concrete fabrication, the geometry of the structure and the relative humidity of the ambient environment.

In the CDP model, the inelastic strain tensor, $\boldsymbol{\varepsilon}^{in}$, takes into account the irreversible inelastic strains, as those arose from concrete cracking. In the case of uniaxial tension, for instance, the equivalent inelastic strain, $\tilde{\varepsilon}^{in}$, is defined in terms of the damage variable as:

$$\tilde{\varepsilon}^{in} = \tilde{\varepsilon}^{ck} - \frac{d}{1-d} \cdot \frac{f_t}{E_0} \tag{12}$$

where $\tilde{\varepsilon}^{ck}$ is the cracking strain (which is irreversible), f_t is the tensile strength, and E_0 is the initial undamaged elastic modulus.

The damage variable, d, is a scalar defined in terms of the effective stress tensor and hardening or softening variables, which can be independently defined for either compression or tension, respectively. These values control the evolution of the yield surface and the degradation of the elastic stiffness, $\mathbf{D}^{el}$. Along with the yield surface function, a flow potential function is required to define the plastic flow. In the present CDP model, a Drucker-Prager hyperbolic function is used for the flow potential (Lubliner et al. 1989; Lee and Fenves 1998).

The thermal expansion strain takes into account the effect of the temperature change in the concrete mix with respect to the room temperature promoted mainly by the hydration process, especially at early ages:

$$\boldsymbol{\varepsilon}^{th} = \alpha(T - T_r)\mathbf{I} \tag{13}$$

where α is the thermal expansion coefficient, T is the temperature field obtained from solving Eq. (6), and $\mathbf{I}$ the identity tensor.

In order to characterize the material response with the use of the CDP model, it is therefore necessary to provide the material elastic constants (i.e., Young's modulus, E, and Poisson's ratio, ν), coefficient of thermal expansion (α), uniaxial tensile behavior in terms of stress-opening (e.g., a linear function defined by the tensile strength, f_t, and fracture energy in mode I, G_F) and damage-opening laws, uniaxial compressive behavior in terms of stress-inelastic crushing strain and damage-inelastic crushing strain laws, and the Drucker–Prager associated parameters (i.e., dilation angle, eccentricity, surface shape parameter, and compressive biaxial to uniaxial strength ratio). This model is available in the commercial software Abaqus (SIMULIA Corp 2016) and more details on its implementation can be found in (Montero-Chacón et al. 2015, 2017).

As explained in the next section, the previous CDP parameters can be defined in terms of the temperature, which is obtained in the thermal analysis, and the curing time. Although early age cracking is a coupled thermo-mechanical problem, the thermal and mechanical problems can be solved in a sequential process as the mechanical dependency of the thermal properties has been assumed negligible. In the cases presented herein, however, the influence of the curing age in the material properties is stronger than that of the temperature as gradients below 30 °C are expected.

2.3 Summary of the Methodology

The model described above allows the estimation of the optimal stripping time for concrete structures considering the cement hydration process and potential early age cracking. We present a methodology for the analysis of early age cracking in large concrete structures by implementing the aforementioned models with the FEM. The procedure consists of the following steps:

- Step 1: Determination of the volumetric heat flux [use Eq. (5)].
- Step 2: Identification of the mechanical properties of the concrete in terms of its age.
- Step 3: Solving of the thermal problem (using the volumetric heat flux from step 2).
- Step 4: Solving of mechanical problem (using T obtained in step 3).
- Step 5: Determination of the stress fields and crack widths (based on equivalent plastic strains).

Cifuentes *et al. Int J Concr Struct Mater*   (2019) 13:41

Page 5 of 20

- Step 6: On-site monitoring (optional) and standard checks.

Step 5 can be implemented within a specific objective function in order to optimize the stripping time, which is already accounted for in the numerical model. This becomes very relevant in the case of large structures where time plays an important role in the cost of the structure and, as is already known, its execution is somehow limited by the curing time.

3 Material Characterization

The two first steps of the methodology require both the determination of the volumetric heat flux and the identification of the mechanical properties of the concrete in terms of its age. Therefore, it is mandatory to characterize the input material parameters used in the present methodology so as to complete the analysis. In this section, we present an experimental approach to the characterization of such properties.

3.1 Measurement of the Heat of Hydration

One of the main aims of the numerical model is to consider the heat of hydration of the cement during the curing process of the concrete. This issue has been analyzed by concreting a 1 m side cube with embedded temperature sensors as described below. Although the heat of hydration of the cement is usually measured under adiabatic or semi-adiabatic conditions (Krauß and Hariri 2006; Schindler and Folliard 2005; Ulm and Coussy 1998), in this case the cube was not isolated, making possible the calibration of the numerical model in a massive element in which the heat of hydration is very high (especially at the center of the cube) and with thermal interaction with the environment in realistic conditions.

The classical method used in curing monitoring are based on the analysis of the temperature profile (Azenha et al. 2009). A non-destructive sensing system has been implemented with a low-cost and compact design, especially suited to be embedded into concrete. Wired sensors have been chosen for the sake of simplicity and in order to gather the information required by the numerical model.

Concrete is an extremely aggressive material at early stages (Neville 1995). Thus, the sensor layer exposed to the surrounding concrete must ensure an accurate measure of the temperature but also be protected from the direct contact. Then, the sensors are placed within freshly poured reinforced concrete and the first signals are checked to ensure that the system can be used from the first pour. The sensors were tested so as to evaluate the suitability of the protection. The results showed no effects

on the response and accuracy of the sensor. The digital temperature sensor DS18B20 (Maxim Integrated, Inc.) has been used. This 1-wire sensor is fairly accurate and can give up to 12 bits of precision. It can work with any microcontroller using a single digital pin, and multiple sensors can be directly connected to the same pin since each one has a unique 64-bit identifier. The sensor covers the range of temperatures for the target application.
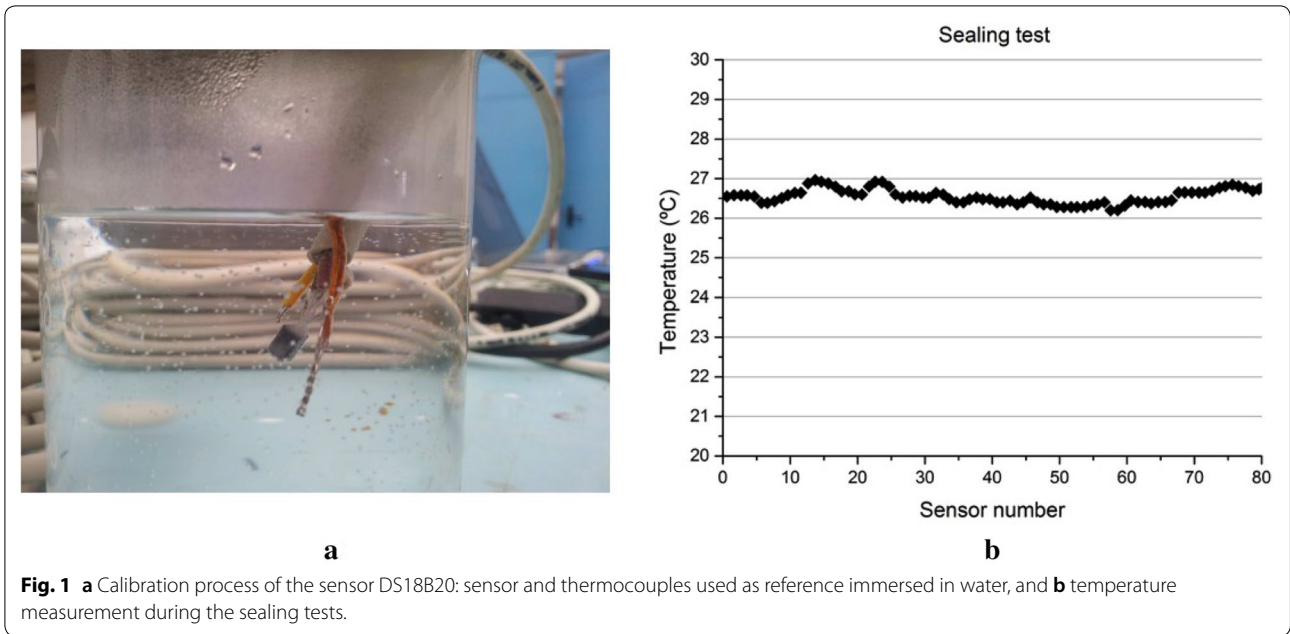
3.1.1 Calibration and Sealing Tests

Preliminary tests were carried out for the characterization and verification of the sensors before placing them into the concrete. The linearity and accuracy of the sensors were compared with two thermocouples. The tests were performed by immersing the sensors in a container with water, as shown in Fig. 1a. It must be noted that water has two main advantages over air: it requires an easier control of the temperature and it shows higher stability. Moreover, it allows checking the proper sealing of the sensors. To protect the sensors and ensure the sealing, they were coated with a special lacquer and resin. The sensor was found to work accurately when compared to the temperature readings of the thermocouples. It must be remarked that the sensor follows a similar evolution to that of the references with an offset of only 0.29 ± 0.5 °C. Figure 1b shows the results of the sealing test performed for 80 sensors. The maximum deviation of the temperature was 0.47 °C and no problems in data communication were detected.

### 3.1.2 Construction Site Conditions

A second test was performed on the sensors which replicates, as closely as possible, on site conditions in order to determine the effects of concrete. Thus, the sensors were deployed inside the pour, and the gathered data was transmitted to the 3PB0012 data acquisition board (Sure-Electronics) governed by a PIC24FJ256GB106 microcontroller located outside the mix.

A 1 m^3 mold was designed using steel backed formwork. The mold was filled with reinforced concrete. This test determines if it is possible to use the sensors inside concrete and check the data transmission. A total amount of 80 sensors were deployed covering the entire volume of the mold as depicted in Fig. 2a, and a total of 4 sensors were placed on each steel bar. Figure 2b shows the final distribution of the sensors tied to the reinforcement bars. For the placement of the sensors a specific part was designed and fabricated using 3D printing. The data acquisition board includes multiplexors and drivers to read the data from the sensors individually.

Figure 3a shows the cast concrete cube without the mold, and some internal and external temperature measurements are shown in Fig. 3b. The temperature profiles
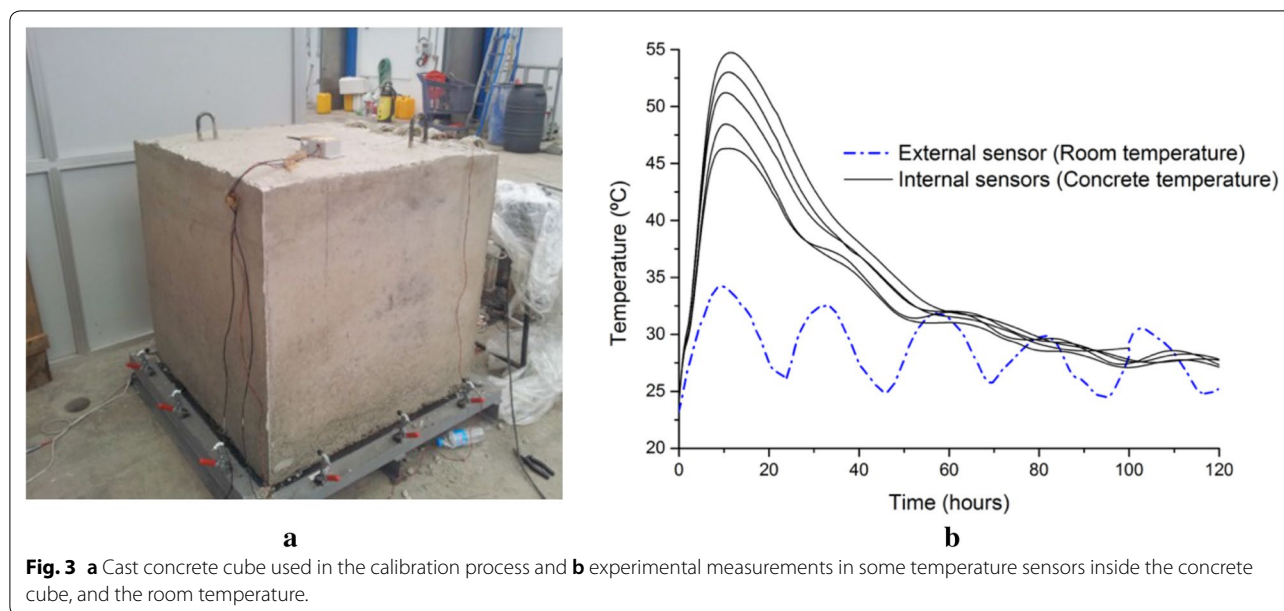
Fig. 1 **a** Calibration process of the sensor DS18B20: sensor and thermocouples used as reference immersed in water, and **b** temperature measurement during the sealing tests.
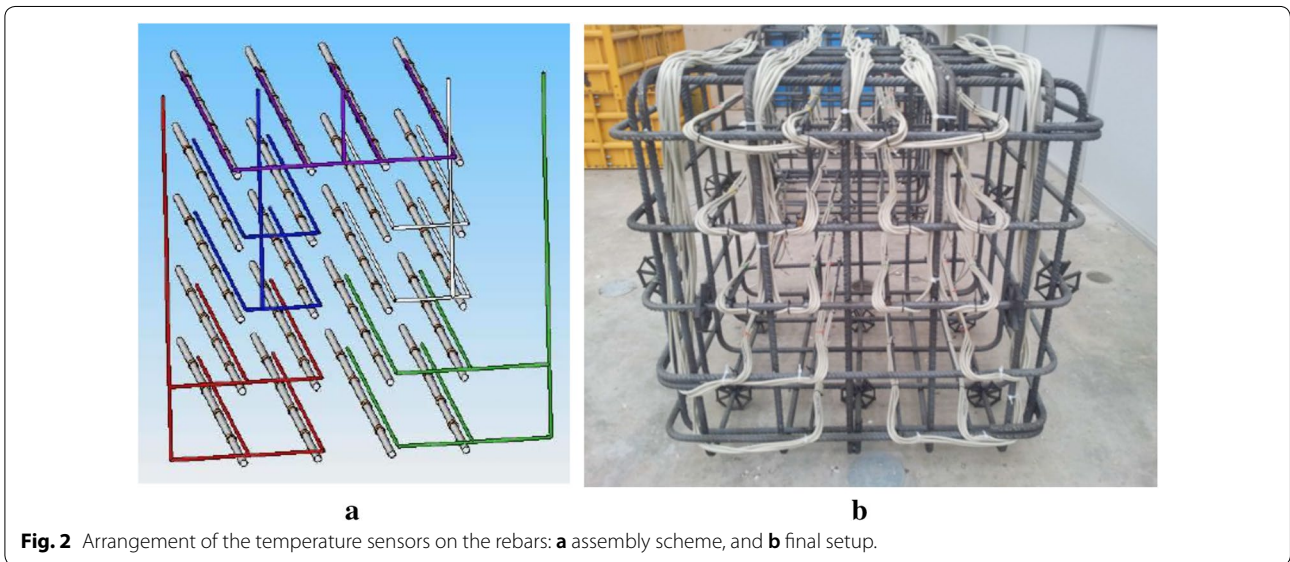
Fig. 2 Arrangement of the temperature sensors on the rebars: **a** assembly scheme, and **b** final setup.

presented in this figure correspond to sensors embedded in the concrete cube at different locations and the room temperature, following the procedure proposed by Azenha et al. (2009). As can be seen in the figure, the temperature increases in the first hours as the cement and water react aggressively, reaching a peak during this time. It must be remarked that some internal sensors reach a temperature lower than others. This is mainly due to the fact that these sensors are located close to the surface, where the heat is dissipated out of the concrete cube. After the first 24 h, the temperature drops, following the fluctuations of the room temperature, as observed in Fig. 3b. It must also be noted that the cube has not been isolated with the purpose of calibrating the numerical model when considering all sorts of external influences. Therefore, the heat dissipation by convective mechanisms through the outer surface can be accounted for.

Fig. 3 **a** Cast concrete cube used in the calibration process and **b** experimental measurements in some temperature sensors inside the concrete cube, and the room temperature.

3.2 Evolution of the Mechanical Properties of Concrete with Age

3.2.1 Elastic Modulus, Compressive Strength, and Tensile Splitting Strength

As pointed out in Sect. 2.2, the mechanical properties required by the CDP model are mostly defined by the uniaxial tension and compression tests, while the biaxial and triaxial tests are required for the definition of the evolution of the yield surface potential.

In this study, we have carried out laboratory tests in order to characterize the uniaxial compressive and tensile behavior of the concrete at different ages. Specifically, we have measured the compressive strength, the Young's modulus, the split tensile strength and the specific fracture energy of the concrete at the ages of 1, 2, 3, 4, 5, 6, 7, 14, 21, and 28 days. In this sense, all the specimens have been made with ready-mix concrete from the same batch. The concrete type used in this study was the one usually employed in construction, with the following weight content ratio of cement/water/sand/gravel/superplasticizer = 1/0.43/2.31/3.07/2.57/0.009. The sand and gravel used in the mix were siliceous aggregates with a maximum size of 16 mm mixed following Fuller's sieve curve. The cement type used for the paste was CEM-II/A-L/42.5R, according to UNE EN197-1:2011, in a 325 kg/m³ dosage. A strict control of the specimen-making process was carried out so as to minimize the scatter in test results. Since the proposed methodology is intended for actual concrete structures, the concrete mix has been supplied by the construction supplier, being the same material as the one employed on the actual construction site.

The characteristic compressive strength (f_c) was determined by means of crushing tests on 100 mm cubes in accordance with UNE EN12930-3:2009. The indirect tensile strength (f_{st}) was obtained through cylinder splitting tests according to UNE EN12930-6:2010. The splitting tests were carried out on 100 mm diameter by 200 mm long cylindrical specimens. The CDP model requires the value of the direct tensile strength (f_t). Since the approach presented herein is for engineering practice purposes, the Model Code approximation (fib CEB-FIP 2012) is used:

$$f_t = 0.9 f_{st} \tag{14}$$

The Young's modulus of the concrete (E_c) was obtained according to UNE EN12390-13:2014 by gradually loading a cylindrical specimen in compression to approximately one-third of its failure load and measuring the corresponding strain. Strain values were measured using two linear variable differential transformer (LVDT) sensors mounted on two concentric steel rings fixed to the concrete specimen and separated 2/3 of the length of the specimen.

The mean values of the measured mechanical properties of the concrete and their deviations are given in Fig. 4, for different ages. It must be remarked that the maximum deviation was of 12% and the results are in agreement with those obtained by other authors (Dao et al. 2009; De Schutter and Taerwe 1997; Kim et al. 2004; Ojdrovic et al. 1987).

As shown in Fig. 4, the experimental results can be accurately fitted by a trilinear curve using the measurements at the ages of 1, 7, and 28 days. This approximation

Cifuentes *et al. Int J Concr Struct Mater*   (2019) 13:41

Page 8 of 20
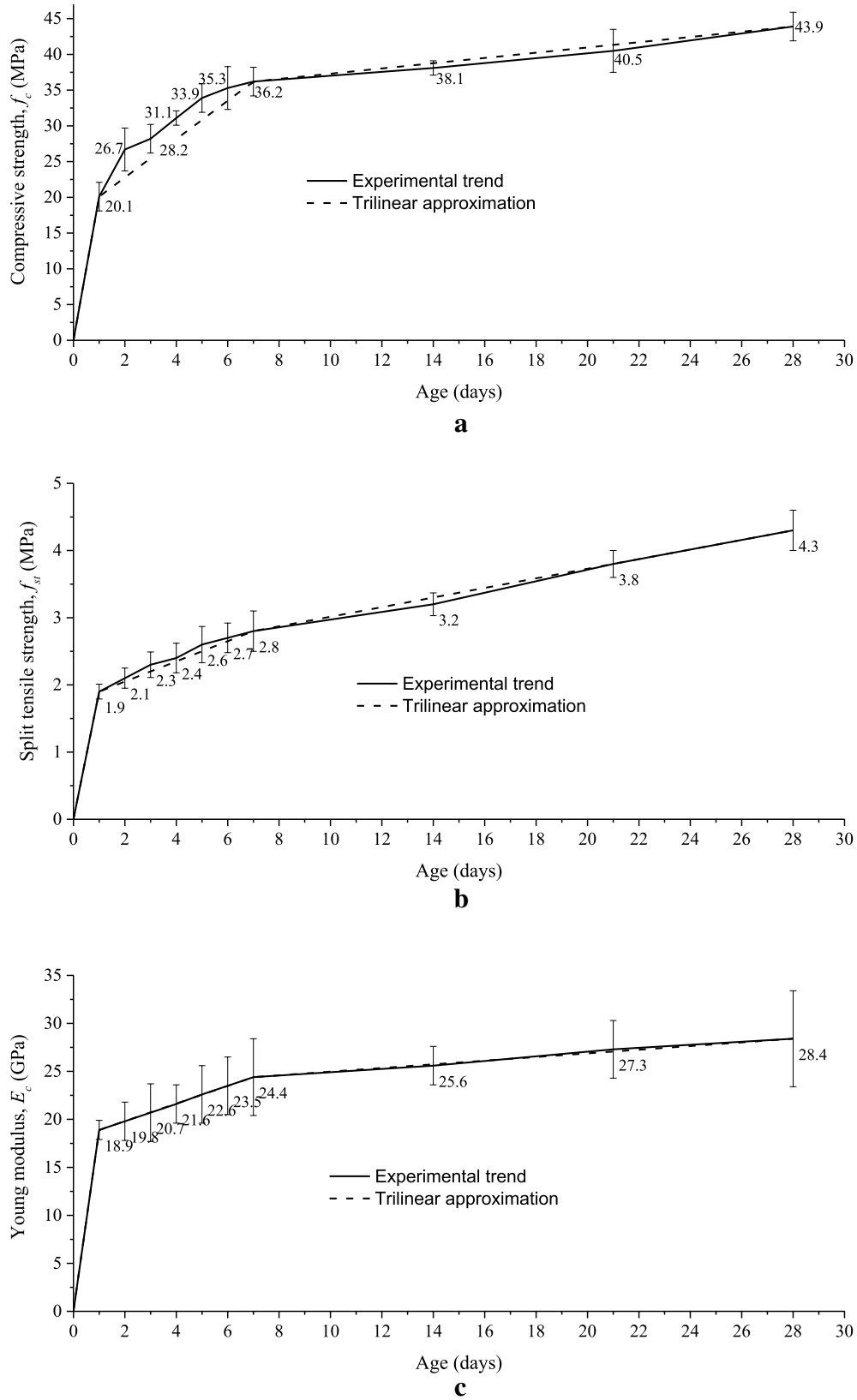
Fig. 4 Evolution of the mechanical properties with age: **a** compressive strength, **b** indirect tensile strength, and **c** Young's modulus.

Cifuentes *et al. Int J Concr Struct Mater*   (2019) 13:41

Page 9 of 20

allows to reduce the number of tests needed to determine the evolution of f_c, f_{st}, and E_c with age. In the case of the Young's modulus (Fig. 4c), the real trend and the trilinear approximation are practically coincident.

Finally, the determination of the parameters describing the flow potential surface (e.g., the Drucker–Prager model) requires bi- and tri-axial tests which are difficult to implement in a structural laboratory (Jankowiak and Łodygowski 2005). However, a global range for the aforementioned parameters, in the case of normal strength concrete, can be found in (SIMULIA Corp 2016). Moreover, a sensitivity analysis of these parameters was carried out and the main conclusion is that the fracture behavior, in the present application, is strongly influenced by the uniaxial behavior.

3.2.2 Fracture Properties

In order to determine a size-independent value of the specific fracture energy of the concrete the simplified boundary effect method proposed by Abadalla and Karihaloo (2003), Karihaloo et al. (2003) has been used. On the basis of this method, the size-independent fracture energy of the concrete is obtained by testing, according to the RILEM three-point bending test (3PBT), two different single size specimens with two different notch-to-depth ratios, provided they are well separated ($a/D = 0.05$ and 0.50). According to this procedure, the size-dependent fracture energy of the concrete (G_f) is obtained for every notch. Then, the boundary effect equations demonstrated by Hu and Wittmann (Cifuentes et al. 2017; Hu and Wittmann 1992) must be applied to each specimen with different notch depth, obtaining a system of two equations and two unknowns, being one of these unknowns the size-independent fracture energy of the concrete, G_F, and the other one the transition length, a_l.

Prismatic notched specimens were subjected to 3PBT according to the experimental requirements of the work-of-fracture method described in the RILEM recommendation (RILEM 1985). The geometric dimensions of the specimens were 100 mm in width, 100 mm in depth, 400 mm of span, and 440 mm in length, with two well-separated relative notch depths of 0.05 and 0.5. Four samples were tested for each notch to depth ratio and age of concrete. The tests were conducted in a ± 25 kN dynamic machine with a closed-loop servo control. The very low rate of loading was controlled by a crack mouth opening displacement (CMOD) gauge so that the fracture occurred in a stable manner. A reference frame with an LVDT displacement transducer was used to measure the vertical displacement at the midpoint of the specimen as seen in Fig. 5. Thus, the load-CMOD (P-CMOD) and load–displacement (P–δ) curves for all specimens were

Fig. 5 Three-point bending test of a notched specimen according to the RILEM work-of-fracture method.

recorded. The supports were of antitorque design, so that any parasitic torque affecting the test specimen was eliminated.

As observed in Fig. 6, the maximum value of the specific fracture energy of the concrete is reached at the age of 2 days. After that, the values of G_F start to decrease slightly. The explanation to this effect is similar to that concerning the fracture behavior of high-strength concrete: when the age of the concrete increases, its compressive strength and Young's modulus also increase. Thus, this means that the older the concrete is, the more effect the cement paste has on its fracture behavior and its stiffness reduces the frictional part originated by the coarse aggregates, which on the other hand provide higher fracture energy values (Cifuentes and Karihaloo 2013). At the age of 1 day, the strength of the concrete is still very low, and this is reflected on its fracture energy. This effect is related with the evolution of the brittle behavior of concrete with age, when the stiffness of the cement paste increases due to the increase of the degree of hydration of the cement.

Figure 7 shows the characteristic length, l_{ch}, obtained as follows:

$$l_{ch} = \frac{E_c G_F}{f_{st}^2} \tag{15}$$

The characteristic length is an important fracture parameter as it establishes a relationship between the three main fracture properties of concrete (Hillerborg et al. 1976). Since l_{ch} is related to the brittleness
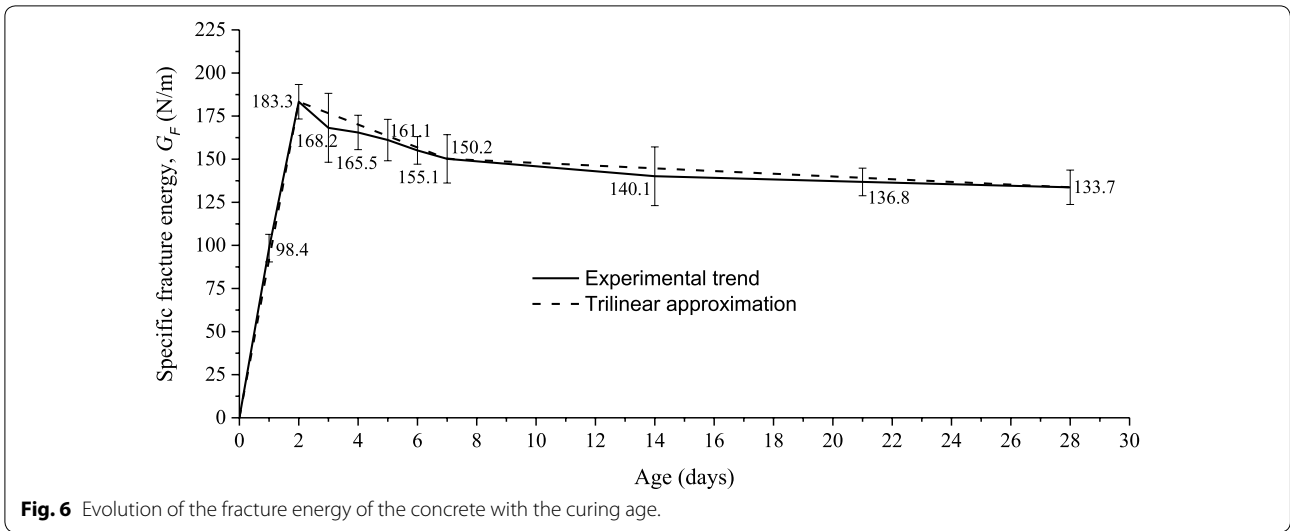
Fig. 6 Evolution of the fracture energy of the concrete with the curing age.
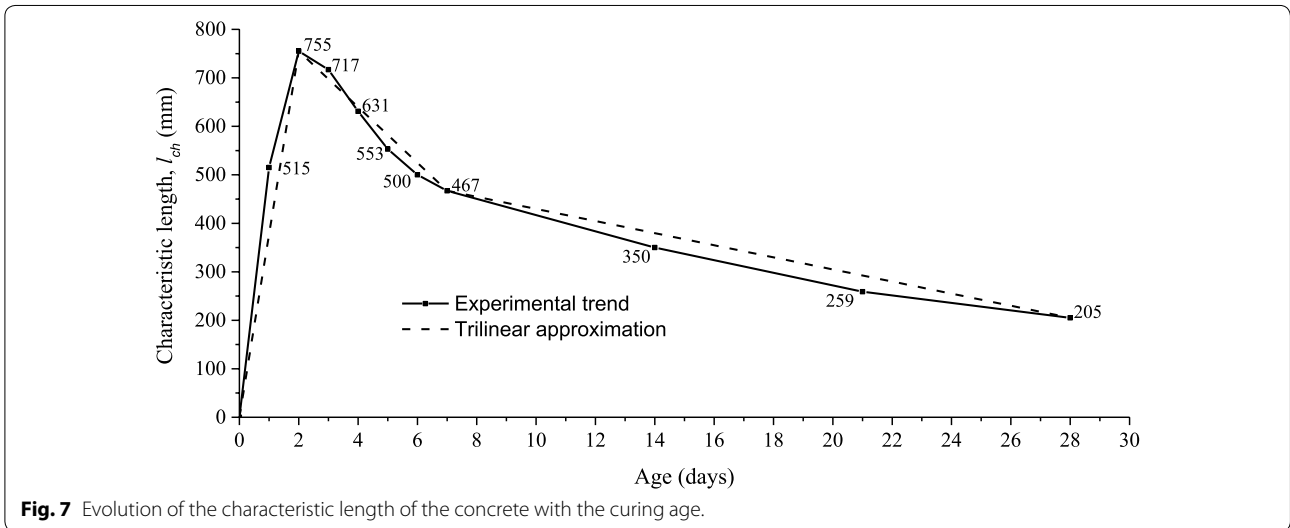
Fig. 7 Evolution of the characteristic length of the concrete with the curing age.

(or ductility) of concrete, it is observed that concrete exhibits a more brittle behavior with age (Cifuentes et al. 2013).

The trilinear approximation shown in Fig. 6 for the variation of G_F and l_{ch} with the age of the concrete is also accurate enough but in this case, since the maximum is obtained at the age of 2 days, the tests at the ages of 2, 7, and 28 days must be carried out.

4 Validation of the Thermo-mechanical Model

Once the mechanical properties of the concrete, in terms of its age, and the volumetric heat flux have been determined by the experimental procedure described above, we can proceed to solve the thermo-mechanical problem, using the methodology presented in

Sect. 2, in order to validate the model. For the widths and materials considered in these applications and due to the careful curing conditions to which the concrete has been subjected (a saturated ambient with water has been maintained), the shrinkage strains can be neglected when compared to those from the thermal expansion. Under other different curing conditions the shrinkage strains of concrete could not be neglected and they must be considered in Eq. (10). Moreover, the tensile strength exhibited by the material after 24 h reached values of 2 MPa, reinforcing the previous assumption. The creep strains have been considered through the creep coefficient, Eq. (11), with a measured relative humidity of the ambient environment of 65%. However, these strains did not generate any damage

to the concrete since the deformations of the material were not impeded, thanks to the geometry and the boundary conditions of the problems analyzed in this paper. In general, creep has to be analyzed rigorously since the thermal gradients originated in concrete produce stresses, which can lead to cracking of the material (see Bazant 1988).

As the reference problem, a 1 m side concrete cube is considered. The cube is subjected to a hydration process and the time-dependent temperature profiles are obtained at the locations of the sensors described in Sect. 3.1.1. These temperature profiles are used in a subsequent thermo-mechanical analysis in order to determine the stress and cracking states, comparing the numerical results with the experimental ones. The numerical simulations were carried out in the commercial FE software Abaqus version 6.12.

4.1 Heat Transfer Model

Since the geometry of the model is very simple (i.e., a regular cube with 1 m side), the discretization of the model is made by regular hexahedral elements with 100 mm sides. Therefore, the model consists of 1000 elements. The element type employed was linear hexahedral for heat transfer, C3D8T.

At this step, only the thermal behavior is analyzed. The cube was cast by pouring the concrete in a mold formed by five metallic wall formworks. The bottom wall is supported on the floor and the lateral sides are in contact with the steel sheets that are subsequently in contact with the air. The top surface of the cube is in direct contact with the environment of the laboratory. Therefore, the thermal boundary conditions in the numerical simulation represent such scenario. In this sense, the bottom concrete surface has a convective steel–concrete boundary condition, as well as the lateral surfaces. However, in the latter case, the formwork is removed after 2 days, and at this point the boundary condition is modified into a convective concrete-air interaction. In the case of the top concrete surface, the boundary condition is kept constant during the entire analysis, considering a convective concrete-air boundary condition. The floor has been modelled with regular four-noded plate elements (R3D4), made of concrete, considering no heat of hydration, and subjected to the room temperature. Table summarizes the input parameters used for the different boundary conditions based on the work by Neville (1995) and Guo et al. (2011).

As pointed out in Sect. 2.3, the heat of hydration of the cement was modeled as a volumetric heat flux following Eq. (5), and is time-dependent. Figure 8 shows the time evolution of the volumetric heat flux Q_h, considered in the thermal problem.

Fig. 8 Time evolution of the volumetric heat flux in the concrete considering the hydration of the cement.
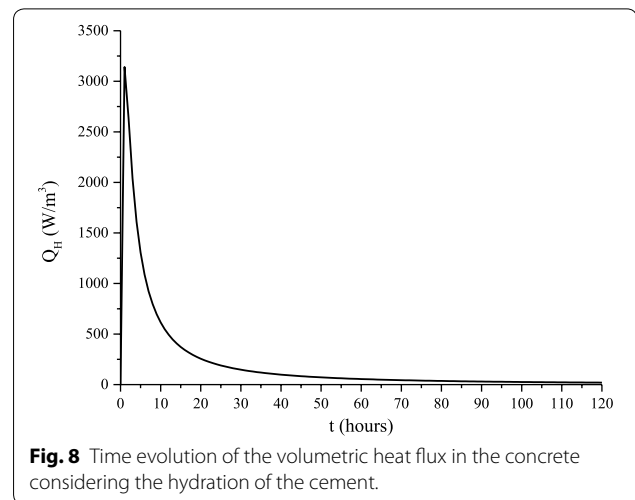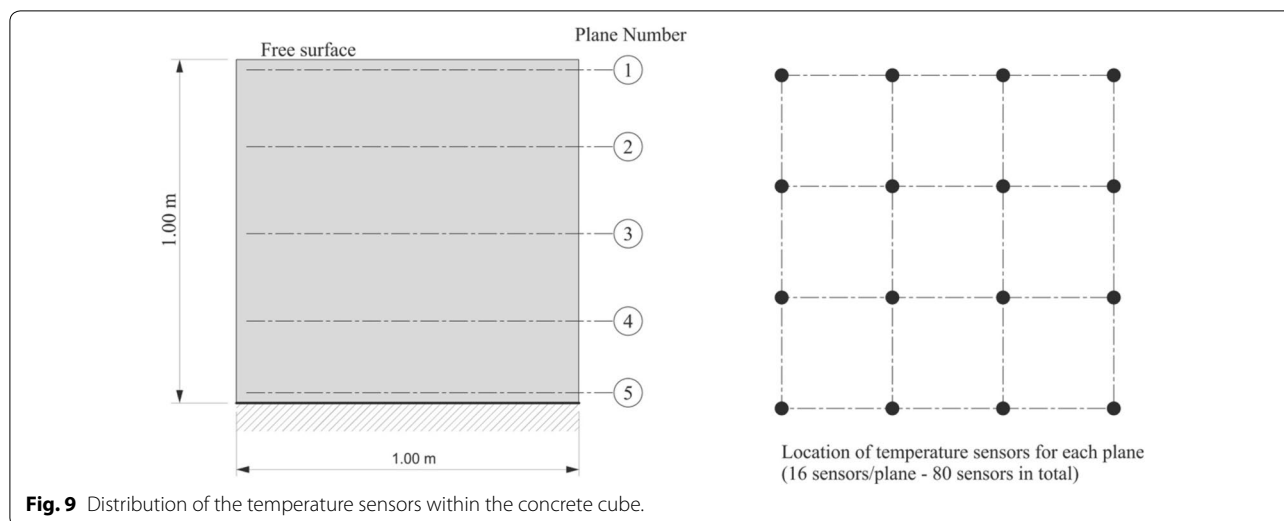
The temperature evolution within the concrete cube during the hydration process was monitored using temperature sensors embedded in the cube, as described in Sect. 3.1. A total of 80 sensors were placed on 5 horizontal planes, as depicted in Fig. 9.

Since there exists a large amount of experimental results, just a few selected sensors where compared with respect to the numerical results in order to calibrate the model. The selected points are those corresponding to the corners of the cube, the half-side, and the center of the cube. These points are very representative since the highest value of the concrete temperature is expected to occur at the center, while the lowest values are expected to appear at the half-side and the corners of the cube. Figure 10 shows the comparison between the numerical and the experimental results, regarding the temperature evolution. The numerical results are in good agreement with the experimental ones; therefore, the heat transfer model is validated.

As observed in Fig. 10, the maximum temperature is reached about 12 h after the casting, and the maximum temperature was recorded at the 4th plane. This is confirmed by the temperature contour plot (see Fig. 11), in which the maximum temperature occurs close to the bottom of the cube, at the 4th plane height.

4.2 Thermo-mechanical Model

Once the temperature distribution has been obtained with the heat transfer model, the thermo-mechanical model is used in order to determine the stress fields and the potential cracking states. Since the model considers the coupling between thermal and mechanical properties and loads, some specific aspects for the stress analysis have been considered in the model. Firstly, the mechanical properties are time-dependent, as determined by the experimental analysis.

Fig. 9 Distribution of the temperature sensors within the concrete cube.

Regarding the boundary conditions, the cube is assumed to be free, only supported on the floor (i.e., the bottom surface). Thus, a steel–concrete contact has been considered with a friction coefficient of $\mu = 0.5$, in accordance with the range proposed by (Baltay and Gjelsvik 1990).

In this calibration problem, the stresses that appear in the cube are promoted by the thermal dilation due to the changes in the temperature caused by the hydration process, and the kinematic constraint by the friction contact between the concrete surfaces and the steel sheets. Figure 12a shows the maximum principal stresses at the maximum temperature instant, which takes place 12 h after the casting process. In this case, the stresses are only due to the cement hydration process and it can be concluded that no (early age) cracking is present as the maximum tensile stress is below the tensile strength. This is in agreement with the experimental observations (Fig. 12b) in which no cracks were found in the cube after 28 days of curing. Finally, from the numerical results (Fig. 12a), it can be observed that the maximum stresses are induced at the edges of the cube because. This is more relevant in the bottom edges due to the friction mechanism between steel and concrete.

5 Applications
In this section we present two applications of the thermo-mechanical model described in Sect. 2, characterized in Sect. 3, and validated in Sect. 4. Both practical cases are referred to retaining walls, yet with different purposes. In the first case, a simple retaining wall is studied with the presented methodology in order to estimate the optimum stripping time. In the second case, the model is applied

to a structure built in Loja (Granada, Spain). The aim of this second analysis is to determine whether an excessive cracking state could be promoted throughout the evolutionary construction phases.

5.1 Estimation of the Optimum Stripping Time in a Retaining Wall
Let us consider a concrete cantilevered retaining wall of 3 m in height, as depicted in Fig. 4, with corrugated steel rebars modeled as embedded elements within the wall. The material properties of the concrete are detailed in the previous sections, while the steel bars have been assumed perfectly elastic plastic with Young's modulus $E_s = 210$ GPa, Poisson's ratio $\nu = 0.3$, and yield stress $f_{ys} = 400$ MPa. The steel properties are time-independent.

In order to assess the retaining capacity and the optimum stripping time, load–displacement curves are obtained for different curing times. For instance, Fig. 13a shows the load–displacement curve, with the displacement measurement at the top of the wall, after 3 days. Additionally, the evolution of the maximum load bearing capacity of the wall (per unit width) has been obtained as well (Fig. 13b). This information is quite relevant when determining the optimum stripping time, and a safety factor must be applied.

Finally, the results obtained with the numerical model can be used to assess the serviceability limit state (SLS) of the wall, as it is able to predict the cracking evolution in the concrete. This analysis is very important, as the breach of this state greatly impairs the durability of the structure. In the next application, an analysis of the cracking state is thoroughly carried out.

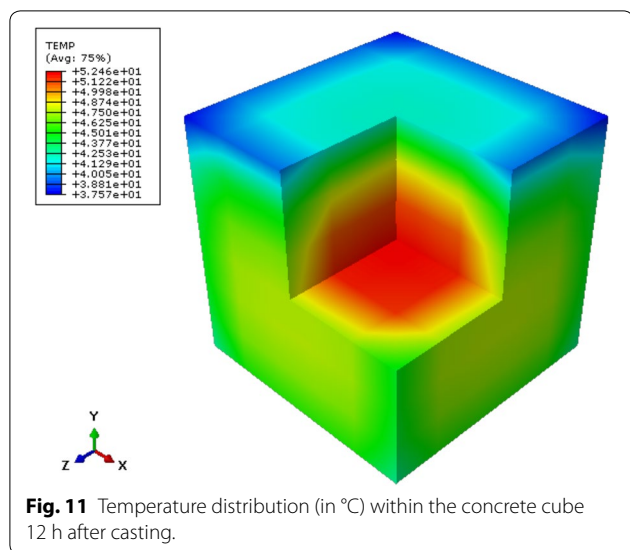Cifuentes *et al. Int J Concr Struct Mater*   (2019) 13:41

Page 13 of 20
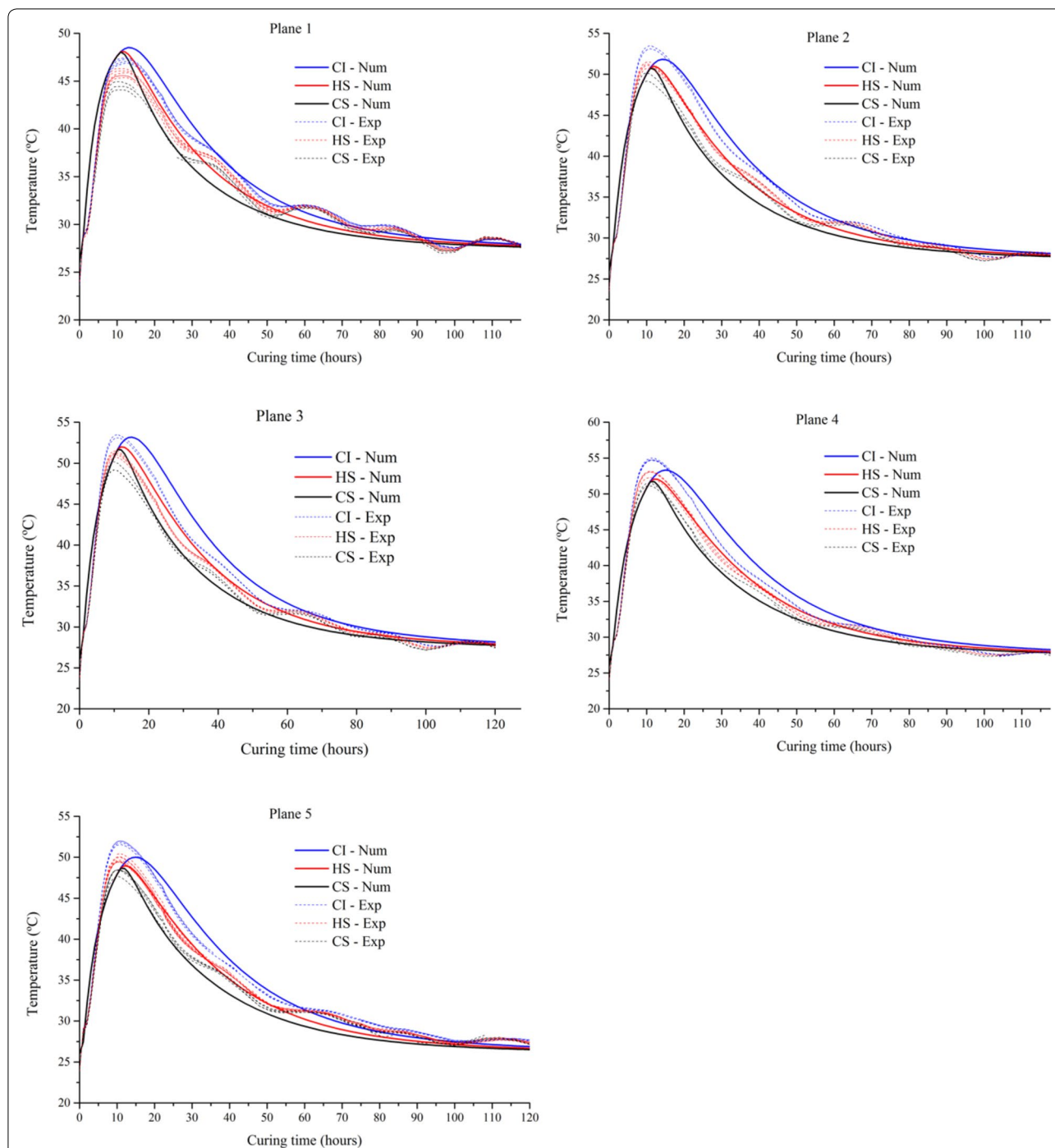
Fig. 10 Comparison of the numerical results for the temperature evolution of the concrete with respect to the experimental results for different sensors at five different planes.

5.2 Analysis of the Staged Construction of a Real Retaining Wall

In this second case, we analyze the step-by-step construction process of a real retaining wall built in Loja (Granada, Spain), shown in Fig. 14. The construction work plan followed by the company consisted of a time difference of 3 days between the casting of the different stages (see Fig. 15a). The soil was poured into the wall 3 days after the concreting of the last stage. In this case, a complete staged construction modelling process has

Cifuentes *et al. Int J Concr Struct Mater* (2019) 13:41

Page 14 of 20

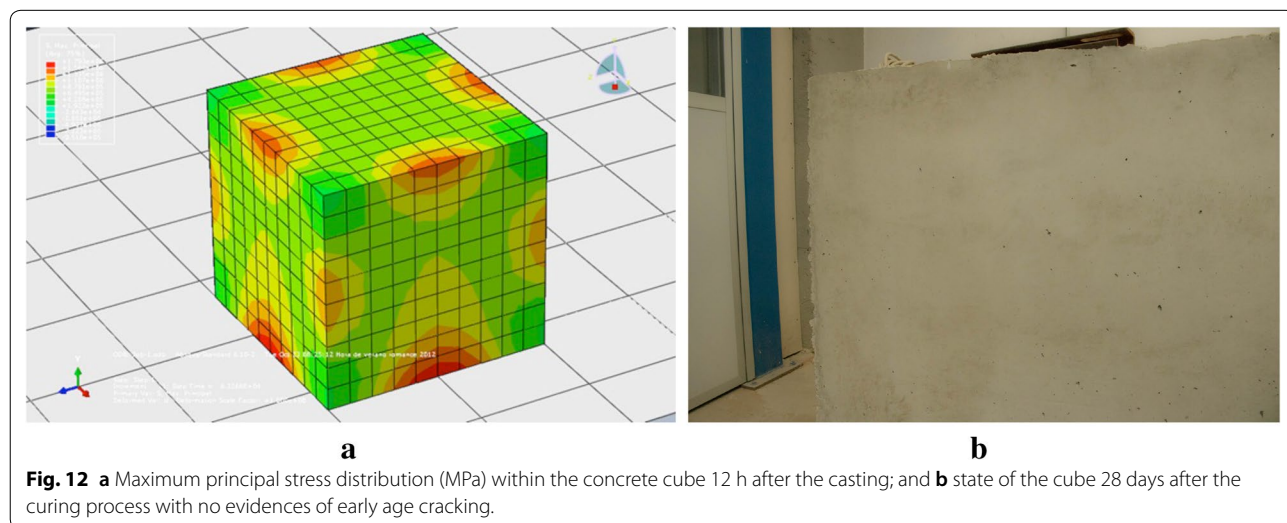**Fig. 11** Temperature distribution (in °C) within the concrete cube 12 h after casting.

been performed, combining the actions of the hydration process of the concrete (with the corresponding evolution of the mechanical properties with age) and the loads corresponding to the construction phases in a time lapse of 3 days according to the construction work plan. Under these considerations, a serviceability limit state (SLS) analysis is carried out in order to validate the proposed construction work plan. Detailed information regarding the geometry and reinforcement of the wall was provided by the company, however, for the sake of simplicity, only a basic geometry scheme is presented in Fig. 15a. Regarding the material properties, the concrete class used onsite is the same that was previously characterized in Sect. 3. Some temperature sensors (sensor S1 to S8 in Fig. 15a) were placed inside the wall before the casting
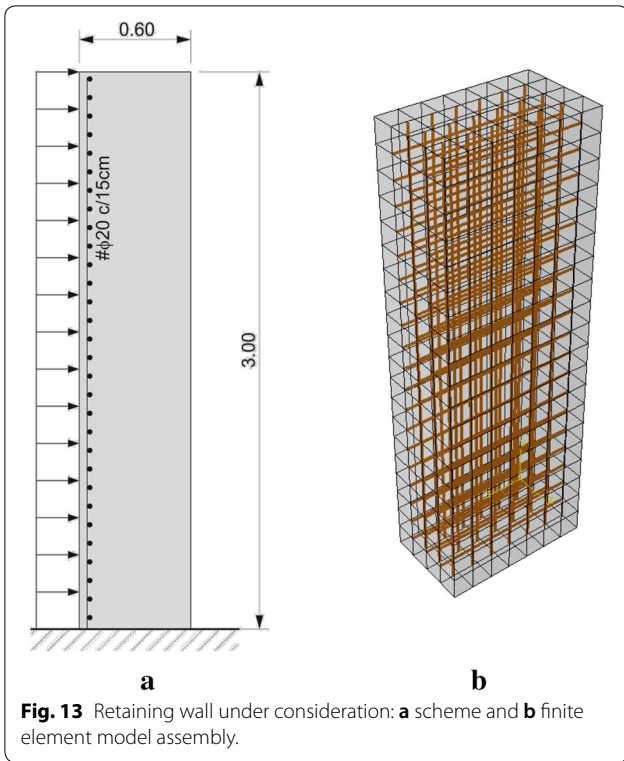
process so as to compare the actual temperature evolution with the model prediction.

The discretization of the geometry consisted in solid temperature-displacement coupled linear hexahedral elements (C3D8T) with a size of 100 mm, approximately (Fig. 16a). The steel rebars are modeled with embedded truss elements (T3D2) with different diameters, namely 10, 12, 16, 25, and 32 mm, and with different spacing between them (Fig. 16b). For geometrical reasons, only a slice of 1 m is considered in the model. The boundary conditions in the inner and outer face of the wall are assumed to be free in the mechanical problem, and a convective mechanism between the surfaces and air are considered for the heat transfer problem by means of a film coefficient. Regarding the foundation, another film coefficient of 2 W/m^{2}K between the concrete and the soil is considered. The air temperature considered for the convective source was the one measured the day previous to the casting process. The measured relative humidity of the ambient environment was 73%. The rest of the thermophysical parameters used in this simulation where those calibrated in Sect. 4 and presented in Table 2.

Regarding the thermo-mechanical analysis, the hydrostatic soil pressure was applied to the external surface of the wall, after 11 days, as described in the construction work plan. The lateral hydrostatic soil pressure was determined using Rankine's theory with active and passive soil coefficients of $K_a = 0.333$ and $K_p = 3.0$, respectively, and a density of $\gamma = 2$ t/m^3 was considered.

In Fig. 17 the temperature distribution predicted by the numerical model of the hydration process is compared with the experimental results recorded by the temperature sensors in the structure. These results are of great interest as they allow for the verification of the hydration

Fig. 12 a Maximum principal stress distribution (MPa) within the concrete cube 12 h after the casting; and **b** state of the cube 28 days after the curing process with no evidences of early age cracking.

Fig. 13 Retaining wall under consideration: **a** scheme and **b** finite element model assembly.

process taking place inside the wall, validating the evolution of the concrete properties with its age.
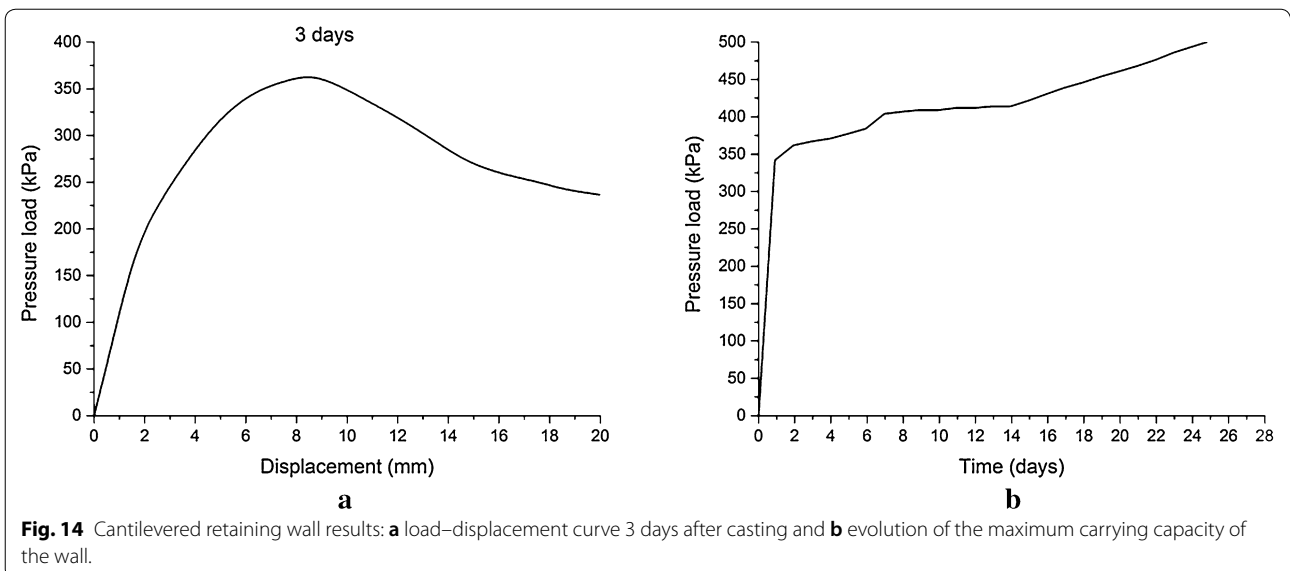
As explained in the previous sections, the temperature distribution is used in the thermo-mechanical analysis in order to assess the stress and cracking states. Thus, the ultimate strength and serviceability limit states, USS and SLS, respectively, can be checked. In this case,

the stripping schedule and the load application were known a priori, hence the compliance of these states at very specific curing times was checked. In this sense, the temperature distribution is presented for ages 3, 11, and 28 days (Fig. 18a–c), with their corresponding stress field along the z-axis (Fig. 18d–f), respectively. The maximum stress reached is below 2.5 MPa, therefore the structure presents an acceptable level of security. For this reason, it can be considered that the stripping time and the work plan are conservative as they do not promote an excessive cracking level as confirmed, on the other hand, by in situ observations at the construction site.

Regarding the USL analysis, the results show that standard requirements are fully complied with. The principal stresses remain below the maximum capacity in the cases of compression and tensile stresses, and the stresses in the steel bars are low, compared to the yield stress of steel. Figure 19a shows the distribution of minimum and maximum principal stresses in the steel rebars.

In order to check the compliance of the SLS of cracking, a measure of the crack opening width is required. However, since the maximum principal stresses throughout the entire analysis of the retaining wall remain below the tensile strength, no cracking states arise in this study. This is in agreement with the in situ observations of the real structure. In any case, and for the sake of completeness, the SLS analysis can be carried out as follows.

The CDP model provides a measure on the equivalent plastic strains, which represent the location of cracks. It must be remarked that this model does not follow a smeared crack approach and, therefore, the displacement jump that takes place in a crack cannot

Fig. 14 Cantilevered retaining wall results: **a** load–displacement curve 3 days after casting and **b** evolution of the maximum carrying capacity of the wall.

Cifuentes *et al. Int J Concr Struct Mater*   (2019) 13:41

Page 16 of 20

Fig. 15 Retaining wall construction in Loja (Granada, Spain): **a** main dimensions of the wall in meters, location of the temperature sensors S1 to S8 and indication of the construction stages and, **b** in situ construction of the wall.

a   **b**
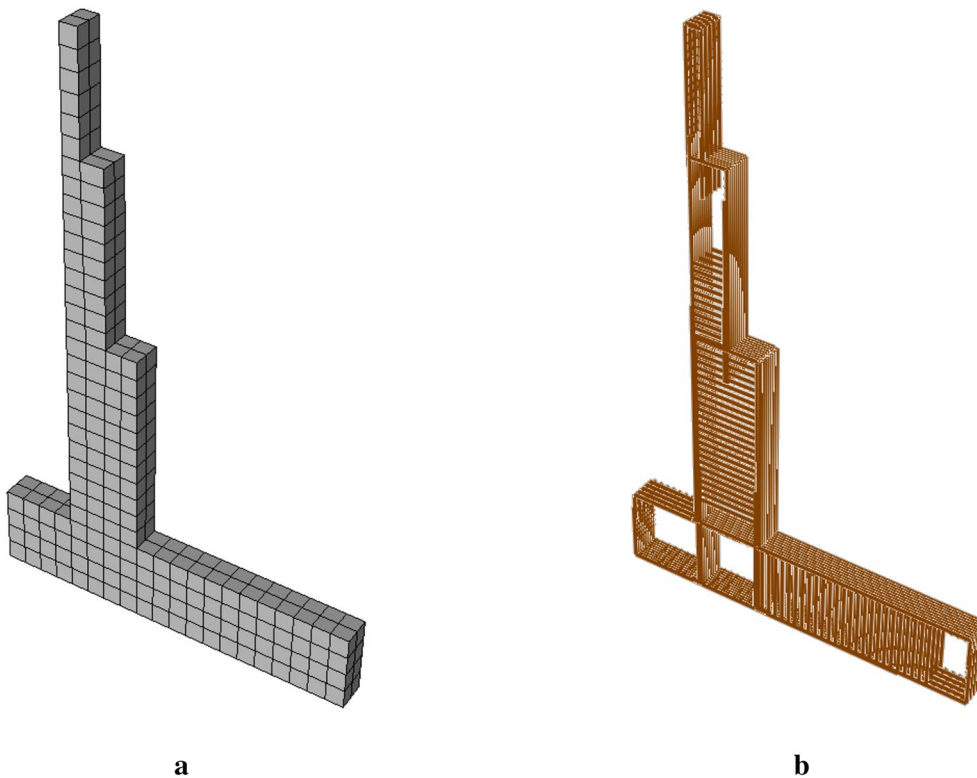
Fig. 16 Finite element model of the retaining wall: **a** C3D8T elements for concrete, and **b** T3D2 elements for the steel rebars.

Cifuentes *et al. Int J Concr Struct Mater* (2019) 13:41

Page 17 of 20

Table 2 Thermophysical parameters considered in the thermal analysis.

Parameter	Value
Density, ρ (kg/m³)	2240
Coefficient of thermal expansion, α (1/K)	10^{-5}
Thermal conductivity, k (W/mK)	2.5
Specific heat, c_p (J/kgK)	922
Film coefficient, concrete-air, h_c (W/m²K)	9
Film coefficient, concrete-formwork, h_{cs} (W/m²K)	1
Room temperature, T_r (°C)	27

be directly measured (SIMULIA Corp 2016). For this reason, the authors suggest the used of inelastic strains (i.e., the equivalent plastic strains, $\tilde{\varepsilon}_t^{pl}$) combined with

the element size (h_{el}), so as to estimate the crack width through the following expression:

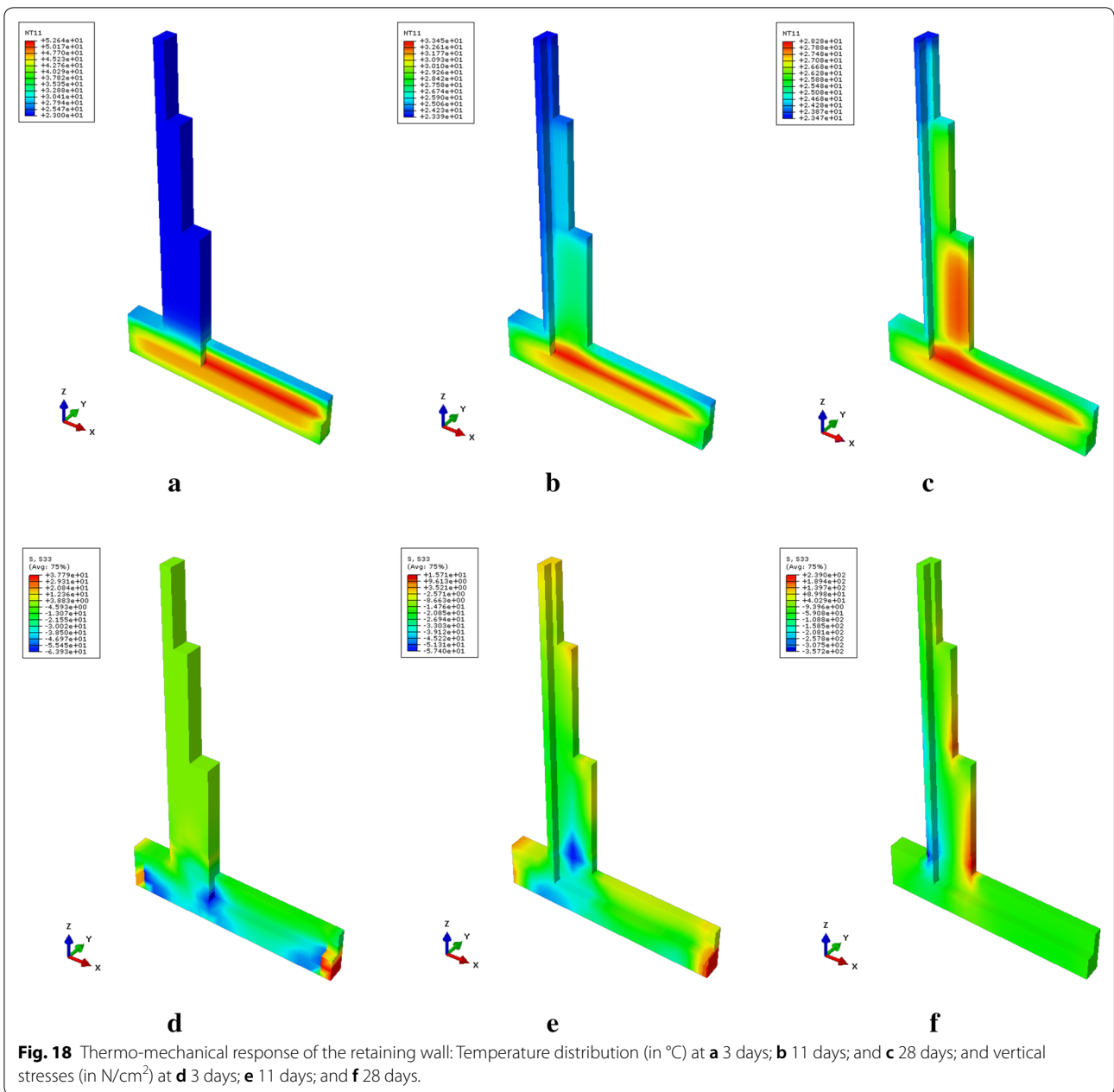$$w \sim h_{el}\tilde{\varepsilon}_t^{pl}. \tag{16}$$

Finally, since the ULS and SLS states have been successfully checked, we can remark that the work plan, especially the stripping time allocation, was appropriate. This was also confirmed by the experimental observations.

6 Conclusions

One of the main problems in the construction of large concrete structures is early age cracking, a phenomenon promoted by the exothermic reaction resulting from cement hydration, which rises the temperature in the mix producing temperature gradients that eventually generate thermal stresses. Moreover, this problem becomes of utmost importance in staged constructions and the
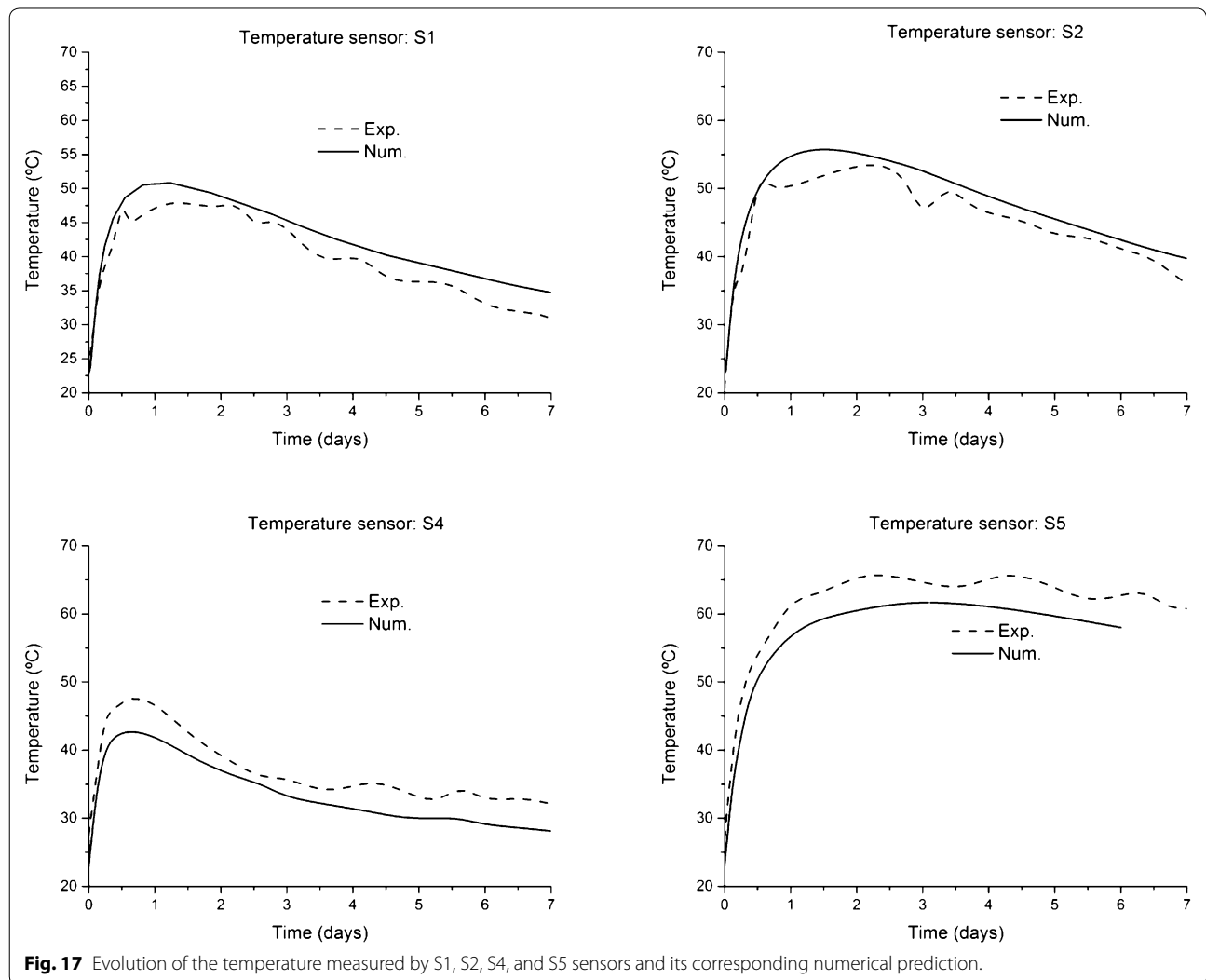
Fig. 17 Evolution of the temperature measured by S1, S2, S4, and S5 sensors and its corresponding numerical prediction.

Fig. 18 Thermo-mechanical response of the retaining wall: Temperature distribution (in °C) at **a** 3 days; **b** 11 days; and **c** 28 days; and vertical stresses (in N/cm²) at **d** 3 days; **e** 11 days; and **f** 28 days.
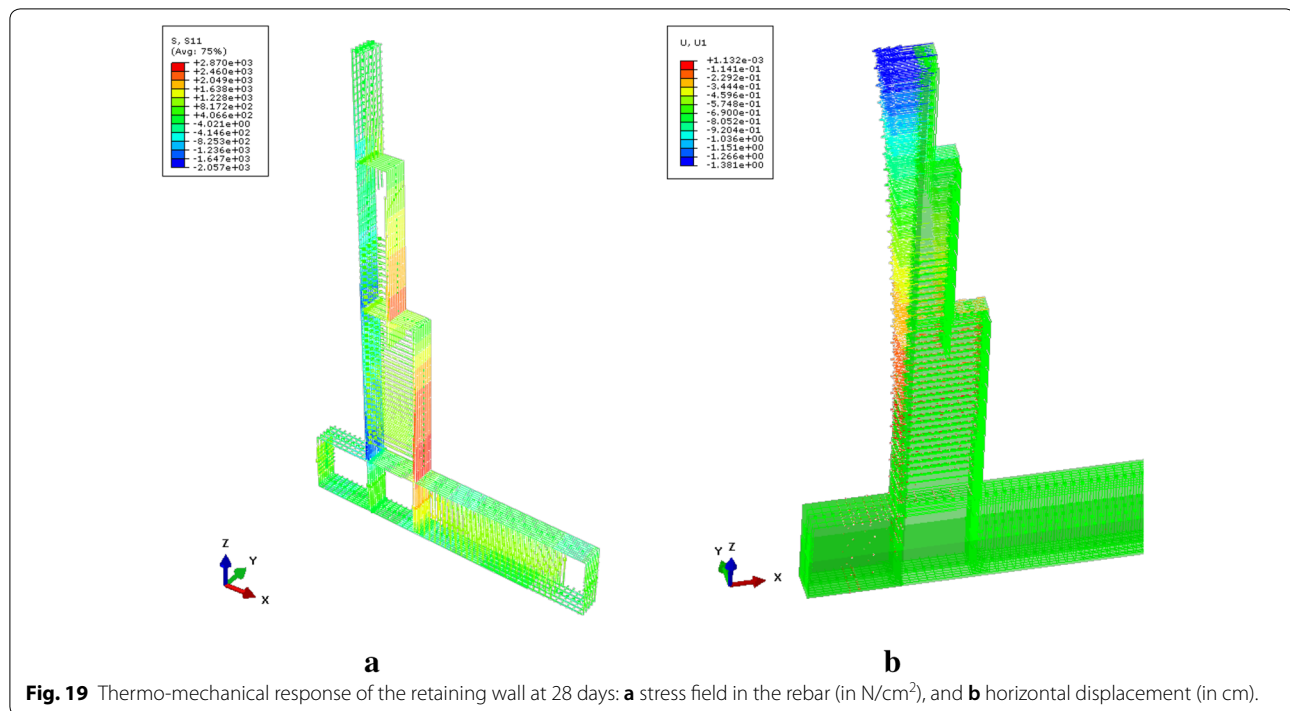
determination of stripping times. Thus, it is evident that a methodology for the determination of the stress and cracking states, so as to check its compliance with respect to the standards, is a demand for civil engineers.

In this work, a finite element-based methodology for the analysis of early age behavior is presented. It consists of two sequentially-coupled models, namely, a heat transfer finite element model used first in order to determine the evolution of the temperature within the concrete mix due to the hydration process, and a subsequent thermo-mechanical finite element model, based on the

continuum damage theory, so as to evaluate the stress and cracking states of the structure.

In order to determine the material properties required by these models, an experimental campaign has been carried out. In the first place, the mechanical properties (i.e., elastic and fracture properties) have been obtained through several tests, showing that trilinear time-dependent functions fit well the mechanical evolution. On the other hand, a new experimental setup was defined in order to monitor the hydration process within the concrete mix in terms of the temperature at different

Cifuentes *et al. Int J Concr Struct Mater*   (2019) 13:41

Page 19 of 20

Fig. 19 Thermo-mechanical response of the retaining wall at 28 days: **a** stress field in the rebar (in N/cm²), and **b** horizontal displacement (in cm).

locations. These experimental results have been used in the validation of the model, and the numerical thermal and mechanical predictions are in agreement with the experimental results and observation.

Finally, the presented methodology has been used for the determination of the optimum stripping time and the thermo-mechanical characterization of evolutionary constructions, namely, a retaining wall site in Loja (Granada, Spain). In this sense, the ULS and SLS states have been properly checked, and the numerical predictions, again, are in agreement with the experimental observations, demonstrating the suitability of our methodology for the analysis of early age assessment in large structures. This methodology is very simple and requires the control of the evolution of the temperature inside the concrete, during the hydration of the cement, as the only verification parameter, resulting in a simple but reliable procedure to be carried out on site and that allows to determine the optimum stripping time of a concrete structure. Future work will be devoted to the optimization of construction times, while reducing the operation and maintenance costs.

Authors' contributions
HC planned the experimental and numerical studies. JG and JC designed the sensors and carried out the experimental measurements of temperature. FM and AM developed the numerical modeling and performed the numerical analysis. All authors contributed to write the paper. All authors read and approved the final manuscript.

Availability of data and materials
All data generated or analysed during this study are included in this published article.

Competing interests
The authors declare that they have no competing interests.

Author details
[1] Dpto. Mecánica de Medios Continuos y Teoría de Estructuras, ETS de Ingeniería, Universidad de Sevilla, Seville, Spain. [2] Dpto. Ingeniería, Universidad Loyola Andalucía, Calle Energía Solar 1, 41014 Seville, Spain. [3] Dpto. Ingeniería Electrónica, Sistemas Informáticos y Automática, Universidad de Huelva, Huelva, Spain. [4] Dpto. Ingeniería Electrónica, ETS de Ingeniería, Universidad de Sevilla, Sevilla, Spain.

References
Abdalla, H. M., & Karihaloo, B. L. (2003). Determination of size-independent specific fracture energy of concrete from three-point bend and wedge splitting tests. *Magazine of Concrete Research, 55*(2), 133–141.
Azenha, M., Faria, R., & Ferreira, D. (2009). Identification of early-age concrete temperatures and strains: Monitoring and numerical simulation. *Cement & Concrete Composites, 31*(6), 369–378. https://doi.org/10.1016/j.cemco ncomp.2009.03.004.

Baltay, P., & Gjelsvik, A. (1990). Coefficient of friction for steel on concrete at high normal stress. *Journal of Materials in Civil Engineering, 2*(1), 46–49. https://doi.org/10.1061/(ASCE)0899-1561(1990)2:1(46).

Bazant, Z. P. (1988). *Mathematical modeling of creep and shrinkage of concrete.* New York: Wiley.

Bergström, S. G., & Byfors, J. (1980). Properties of concrete at early ages. *Matériaux et Construction, 13*(3), 265–274. https://doi.org/10.1007/BF02473566.

Bernard, O., Ulm, F. J., & Lemarchand, E. (2003). A multiscale micromechanics-hydration model for the early-age elastic properties of cement-based materials. *Cement and Concrete Research, 33*(9), 1293–1309. https://doi.org/10.1016/S0008-8846(03)00039-5.

Cifuentes, H., García, F., Maeso, O., & Medina, F. (2013). Influence of the properties of polypropylene fibres on the fracture behaviour of low-, normal- and high-strength FRC. *Construction and Building Materials, 45,* 130–137.

Cifuentes, H., & Karihaloo, B. L. (2013). Determination of size-independent specific fracture energy of normal- and high-strength self-compacting concrete from wedge splitting tests. *Construction and Building Materials, 48,* 548–553.

Cifuentes, H., & Karihaloo, B. L. (2018). Analysis of the early-age cracking in concrete made from rapid hardening cement. *Hormigón y Acero, 69*(285), 101–112. https://doi.org/10.1016/j.hya.2018.02.002.

Cifuentes, H., Lozano, M., Holusova, T., Medina, F., Seitl, S., & Fernandez-Canteli, A. (2017). Modified disk-shaped compact tension test for measuring concrete fracture properties. *International Journal of Concrete Structures and Materials, 11*(2), 215–228. https://doi.org/10.1007/s40069-017-0189-4.

Chaboche, J. L. (1988). Continuum damage mechanics. Part I-general concepts. *Journal of Applied Mechanics, 55*(1), 59–64. https://doi.org/10.1115/1.3173661.

Corp, S. I. M. U. L. I. A. (2016). *Abaqus analysis user's guide.* Johnston: SIMULIA Corp.

Dao, V. T. N., Dux, P. F., & Morris, P. H. (2009). Tensile properties of early-age concrete. *Materials Journal, 106*(6), 483–492.

De Schutter, G., & Taerwe, L. (1997). Fracture energy of concrete at early ages. *Materials and Structures, 30,* 67–71.

Faria, R., Azenha, M., & Figueiras, J. A. (2006). Modelling of concrete at early ages: Application to an externally restrained slab. *Cement & Concrete Composites, 28*(6), 572–585. https://doi.org/10.1016/j.cemconcomp.2006.02.012.

fib CEB-FIP. (2012). *fib Bulletin No. 65: Model code for concrete structures 2010.* https://www.fib-international.org/publications/fib-bulletins/model-code-2010-final-draft,-volume-1-detail.html

Guo, L., Guo, L., Zhong, L., & Zhu, Y. (2011). Thermal conductivity and heat transfer coefficient of concrete. *Journal of Wuhan University of Technology-Material Science Edition, 26*(4), 791–796. https://doi.org/10.1007/s11595-011-0312-3.

Hattel, J. H., & Thorborg, J. (2003). A numerical model for predicting the thermomechanical conditions during hydration of early-age concrete. *Applied Mathematical Modelling, 27*(1), 1–26. https://doi.org/10.1016/S0307-904X(02)00082-3.

Hillerborg, A., Modéer, M., & Petersson, P. E. (1976). Analysis of crack formation and crack growth in concrete by means of fracture mechanics and finite elements. *Cement and Concrete Research, 6,* 773–782.

Hu, X. Z., & Wittmann, F. H. (1992). Fracture energy and fracture process zone. *Materials and Structures, 25*(6), 319–326.

Jankowiak, T., & Łodygowski, T. (2005). Identification of parameters of concrete damage plasticity constitutive model. *Foundations of Civil and Environmental Engineering, 6,* 53–69.

Kachanov, M. (1980). Continuum model of medium with cracks. *Journal of the Engineering Mechanics Division, 106*(5), 1039–1051.

Karihaloo, B. L., Abdalla, H. M., & Imjai, T. (2003). A simple method for determining the true specific fracture energy of concrete. *Magazine of Concrete Research, 55*(5), 471–481.

Kim, J.-K., Lee, Y., & Yi, S.-T. (2004). Fracture characteristics of concrete at early ages. *Cement and Concrete Research, 34*(3), 507–519. https://doi.org/10.1016/j.cemconres.2003.09.011.

Krauß, M., & Hariri, K. (2006). Determination of initial degree of hydration for improvement of early-age properties of concrete using ultrasonic wave propagation. *Cement & Concrete Composites, 28*(4), 299–306. https://doi.org/10.1016/j.cemconcomp.2006.02.007.

Kwan, A. K. H., & Ma, F. J. (2017). Two-dimensional early thermal crack analysis of concrete structures by finite element method. *Engineering Structures, 143,* 1–10. https://doi.org/10.1016/j.engstruct.2017.04.005.

Lee, J., & Fenves, G. L. (1998). Plastic-damage model for cyclic loading of concrete structures. *Journal of Engineering Mechanics, 124*(8), 892–900. https://doi.org/10.1061/(ASCE)0733-9399(1998)124:8(892).

Lee, Y., & Kim, J.-K. (2009). Numerical analysis of the early age behavior of concrete structures with a hydration based microplane model. *Computers & Structures, 87*(17–18), 1085–1101. https://doi.org/10.1016/j.compstruc.2009.05.008.

Lee, C., Lee, S., & Nguyen, N. (2016). Modeling of compressive strength development of high-early-strength-concrete at different curing temperatures. *International Journal of Concrete Structures and Materials, 10*(2), 205–219. https://doi.org/10.1007/s40069-016-0147-6.

Lubliner, J., Oliver, J., Oller, S., & Oñate, E. (1989). A plastic-damage model for concrete. *International Journal of Solids and Structures, 25*(3), 299–326. https://doi.org/10.1016/0020-7683(89)90050-4.

Mihashi, H., & de Leite, J. P. (2004). State-of-the-art report on control of cracking in early age concrete. *Journal of Advanced Concrete Technology, 2*(2), 141–154. https://doi.org/10.3151/jact.2.141.

Montero-Chacón, F., Cifuentes, H., & Medina, F. (2017). Mesoscale characterization of fracture properties of steel fiber-reinforced concrete using a lattice-particle model. *Materials, 10*(2), 207. https://doi.org/10.3390/ma10020207.

Montero-Chacón, F., Schlangen, E., Cifuentes, H., & Medina, F. (2015). A numerical approach for the design of multiscale fibre-reinforced cementitious composites. *Philosophical Magazine, 95*(28–30), 3305–3327. https://doi.org/10.1080/14786435.2015.1040101.

Neville, A. M. (1995). *Properties of concrete* (4th ed.). Harlow: Longman Group UK Limited.

Newell, S., & Goggins, J. (2018). Investigation of thermal behaviour of a hybrid precasted concrete floor using embedded sensors. *International Journal of Concrete Structures and Materials, 12*(1), 66. https://doi.org/10.1186/s40069-018-0287-y.

Ojdrovic, R. P., Stojimirovic, A. L., & Petroski, H. J. (1987). Effect of age on splitting tensile strength and fracture resistance of concrete. *Cement and Concrete Research, 17*(1), 70–76. https://doi.org/10.1016/0008-8846(87)90060-3.

Park, G.-K., & Yim, H. J. (2017). Evaluation of fire-damaged concrete: An experimental analysis based on destructive and nondestructive methods. *International Journal of Concrete Structures and Materials, 11*(3), 447–457. https://doi.org/10.1007/s40069-017-0211-x.

Poole, J. L. (2007). *Modeling temperature sensitivity and heat evolution of concrete.* Austin: The University of Texas at Austin.

RILEM. (1985). TCM-85: Determination of the fracture energy of mortar and concrete by means of three-point bend tests on notched beams. *Materials and Structures, 18*(106), 287–290.

Schindler, A. K., & Folliard, K. J. (2005). Heat of hydration models for cementitious materials. *ACI Materials Journal, 102*(1), 24–33.

Ulm, F.-J., & Coussy, O. (1995). Modeling of thermochemomechanical couplings of concrete at early ages. *Journal of Engineering Mechanics, 121*(7), 785–794. https://doi.org/10.1061/(ASCE)0733-9399(1995)121:7(785).

Ulm, F.-J., & Coussy, O. (1998). Couplings in early-age concrete: From material modeling to structural design. *International Journal of Solids and Structures, 35*(31–32), 4295–4311. https://doi.org/10.1016/S0020-7683(97)00317-X.

van Breugel, K. (1998). *Prediction of temperature development in hardening concrete.,* RILEM report 15 London: E&FN Spon.

Wang, X. Y., & Lee, H. S. (2010). Modeling the hydration of concrete incorporating fly ash or slag. *Cement and Concrete Research, 40*(7), 984–996. https://doi.org/10.1016/j.cemconres.2010.03.001.

Wang, X. Y., & Luan, Y. (2018). Modeling of hydration, strength development, and optimum combinations of cement-slag-limestone ternary concrete. *International Journal of Concrete Structures and Materials, 12,* 1. https://doi.org/10.1186/s40069-018-0241-z.

Wu, S., Huang, D., Lin, F. B., Zhao, H., & Wang, P. (2011). Estimation of cracking risk of concrete at early age based on thermal stress analysis. *Journal of Thermal Analysis and Calorimetry, 105*(1), 171–186. https://doi.org/10.1007/s10973-011-1512-y.

Publisher's Note